Materials Advances

ROYAL SOCIETY OF CHEMISTRY

PAPER

View Article Online
View Journal | View Issue

Cite this: *Mater. Adv.*, 2022, 3, 5344

Light induced quasi-Fermi level splitting in molecular semiconductor alloys†

Nakul Jain,[a] Rishabh Saxena,[a] Sumukh Vaidya,[a] Wenchao Huang,[b] Adam Welford,[b] Christopher R McNeill[b] and Dinesh Kabra*[a]

Quasi-Fermi-level (QFL) splitting is a direct measure of the open-circuit voltage (V_{OC}) in an optically illuminated semiconductor solar cell (SC). The evolution of QFL splitting under 1 sun illumination in ternary blends of Gaussian disordered (GD) excitonic molecular semiconductors (MSs) is a complex process. The experimental diagonal band-gap (E_{CT}) fitted with Vegard's law provided a bowing parameter as low as 0.05 for the used ternary alloys as a function of the mixing of two n-type semiconductors, which is a hallmark of good mixing without much alloying disorder. An analytical model based on population occupancy in GD systems is used to determine the change in QFLs as a function of the alloy composition in ternary (two n-type and one p-type) MS blends under 1 sun light illumination. The model predicts a remarkable quantitative change in the QFL due to light-induced charge carriers in such alloys to fit the experimental V_{OC} value. This analytical model, combined with temperature-dependent mobility studies on unipolar devices with various MS alloy compositions, also reveals an interesting observation that a suitable change in QFL is due to the formation of an effective density of states (DOS) between the two n-type MSs. Further, a simpler routinely used double-diode model is also used for comparison with the Gaussian disorder model to fit the V_{OC} values of ternary-alloy-based organic solar cells (OSCs). We show that, overall, the model is more generalized for use with any binary and ternary MS heterojunction systems being used for photovoltaic applications to determine the QFL splitting.

Received 6th February 2022,
Accepted 27th April 2022

DOI: 10.1039/d2ma00131d

rsc.li/materials-advances

Introduction

Excitonic molecular semiconductors (MSs) with Gaussian disorder are unconventional compared to commonly used crystalline inorganic semiconductors; hence different mechanisms are required to explain the charge-transport and photo-physical properties of such materials.[1,2] In particular, for the case of photovoltaic devices—where great progress has been made recently with single-junction efficiencies going beyond 18%[3]—an elaborate fundamental-level physical model needs to be developed to explain their operation. The photo-physics of voltage losses is a heavily discussed topic in the solar cell community,[4] and is particularly crucial when excitonic materials are employed.[5,6] MSs require solar cell physics which includes the excitonic state as the intermediate state for the generation of free carriers, as it imposes a revised fundamental Shockley–Queisser limit[7] and a revised ideal-diode equation to get a clear physical picture.[8] Excitonic MS solar cells generally utilize a mixture of two (or three) materials in the form of a bulk heterojunction (BHJ): at least one with a high ionization potential (called the donor) and the other with a high electron affinity (called the acceptor). Exciton dissociation is facilitated by photo-induced charge transfer at the donor (D)/acceptor(A) interfaces, with a high interfacial area overcoming the limited diffusion length of optically generated excitons.[9] Intriguingly, recent studies have suggested that ternary mixtures of these materials might create optimal devices.[10] Understanding such ternary BHJ systems is extremely challenging, with each individual system having its own energetic disorder (σ), electronic band-gap, charge-transport properties, compositional disorder, and interfacial states.[11,12]

Significant efforts have been made to design single-junction BHJ solar cells by adding a third component for improved solar cell performance.[13,14] Certain criteria have been put forward regarding the selection of the material for the third component (donor or acceptor) in these ternary blend systems, including: (i) complementary absorption,[15–17] (ii) favorable solid state packing[10,18,19] to suppress recombination, and (iii) appropriate energy levels to reduce voltage losses[20–22] and the

[a] *Department of Physics, Indian Institute of Technology Bombay, Powai, Mumbai-400076, India. E-mail: dkabra@iitb.ac.in*
[b] *Department of Materials Science and Engineering, Monash University, Wellington Road, Clayton, VIC 3800, Australia*

† Electronic supplementary information (ESI) available. See DOI: https://doi.org/10.1039/d2ma00131d

complementary photovoltaic parameters for two binary extreme solar cells.[23–25] The tunable V_{OC} in a ternary solar cell are in general fitted using a parallel-diode-type model. This model is based on the assumption (D:A_1:A_2) that the two acceptor systems do not interact electrically at all and behave as separate donor–acceptor systems within the bulk heterojunction despite the mixing.[26] Such a model also excludes the possibility of cascade transfer of charge carriers.[27] This is hence an unrealistic picture, since it ignores the significant interactions between both the acceptors and between the acceptors and the donor on account of the mixing, which can introduce significant compositional disorder, a revised effective joint DOS, and energetic disorder of individual components.[28] These are the basic ingredients which are required to understand QFL splitting in any semiconductor material being used as an absorber in a photovoltaic device. It is pretty evident that a tunable V_{OC} can be realized by choosing either systems of two donors with one acceptor or systems of one donor with two acceptors. Mollinger *et al.*, for example, reported the tuning of V_{OC} for a system with one donor and two acceptors,[29] while Felekidis *et al.* demonstrated a tunable V_{OC} by using two donors with one acceptor, explaining this observation with a state-filling model using Gaussian disorder.[30] Considering the growing interest in ternary systems,[13,31] detailed experimental studies combined with an analytical understanding of solar cell device physics in such systems are essential for better insight into and further development of this field.

In this report, we have chosen a system with one p-type, referred to as a donor in the MS (PTB7-Th; D) and two n-type, referred to as acceptors in MS ($PC_{71}BM$, long-range ordered MS;[32] A_1 as acceptor-1 and $IC_{61}BA$, amorphous MS;[33] A_2 as acceptor-2), D:A_1:A_2, to study the light-induced quasi-Fermi-level (QFL) splitting as a function of acceptor composition. Both n-type MSs (A_1 & A_2) form type II heterojunctions with D, and it could be expected that the observed V_{OC} would be dictated by the minimum diagonal band-gap of the D:A_1 system; however, a monotonic change in V_{OC} with a change in the A_1 *vs.* A_2 ratio has been observed (Fig. 1) by us and by others.[24,25] An analytical model based on the population occupancy of light-induced fermions in a Gaussian disordered broadened joint DOS for an MS alloy is utilized with most parameters experimentally determined to gain insights into the MS semiconductor physics of these ternary alloys.[30,34,35] A quantitative change in the light-induced QFL of holes and electrons was determined using our analytical model with experimentally determined semiconductor parameters. We believe the framework of this study to be applicable beyond V_{OC} fitting and to be capable of providing useful insights into the photo-physics and charge transport physics of MSs.[36]

Results

Fig. 1a presents the molecular structures of PTB7-Th (D), $PC_{71}BM$ (A_1) and ICBA (A_2). The work functions of the electrodes and energy levels corresponding to the organic semiconductors (highest occupied molecular orbital (HOMO) and lowest unoccupied molecular orbital (LUMO)) and interlayers are depicted in Fig. 1b.[37–41] The illuminated *J*–*V* characteristics of D:A_1:A_2 solar cells with different ratios of A_1 : A_2 (100 : 0, 90 : 10, 70 : 30, 40 : 60, 20 : 80, 0 : 100) are shown in Fig. 1c. Parameters such as short circuit current J_{SC}, V_{OC}, fill factor (FF) and power conversion efficiency (PCE) are extracted from the illuminated *J*–*V* characteristics (Table S1, ESI†). V_{OC} is

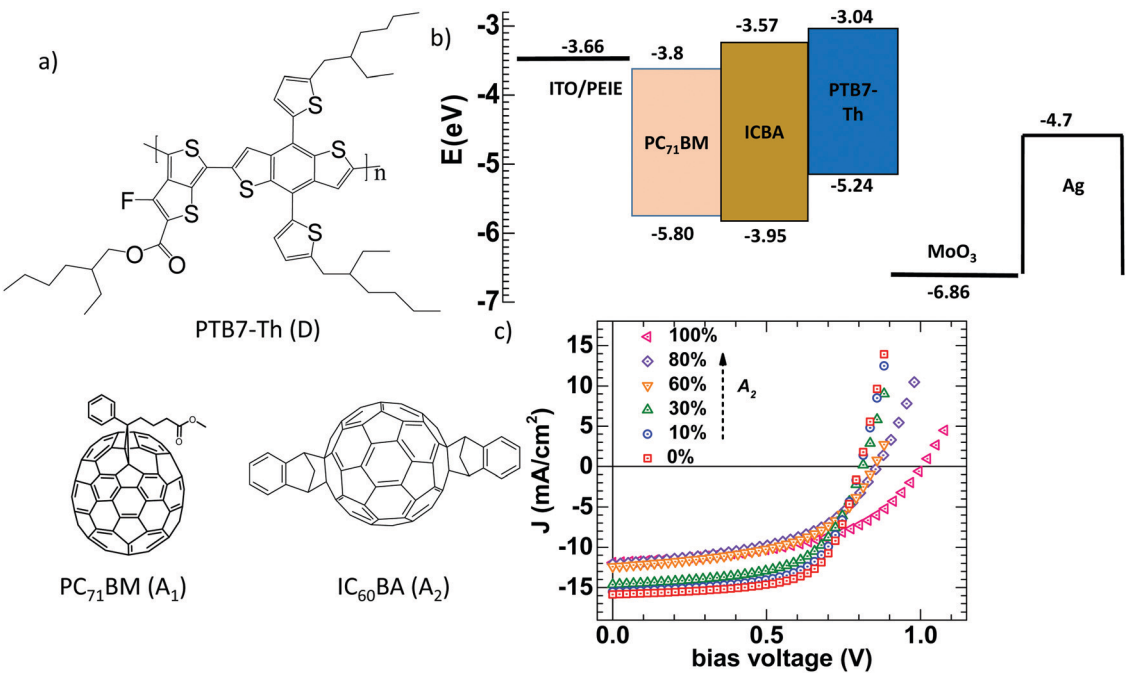

Fig. 1 (a) The molecular structures of D, A_1, and A_2; (b) the device structure with the HOMO and LUMO energy levels (A_1 and A_2,[35] D[33]) and work functions of various layers; and (c) illuminated *J*–*V* characteristics for different A_1 : A_2 ratios in D polymer based solar cells under AM1.5 illumination.

found to vary from 0.80 V (0% A_2) to 0.81 V (10% A_2), 0.82 V (30% A_2), 0.86 V (60% A_2), 0.89 V (80% A_2) and to 1.01 V for 100% A_2. Clearly, V_{OC} is monotonically tuned towards higher values with increasing A_2 concentration and reaches its maximum when there is no A_1 present.[42,43] The total change in V_{OC} is found to be 210 mV in going from 0% A_2 to 100% A_2 in this ternary BHJ system. J_{SC} and FF are also found to vary from 16.1 mA cm^{-2} (0% A_2) to 12.0 mA cm^{-2} (100% A_2), and from 66% (0% A_2) to 51% (100% A_2). The corresponding PCE for the 0% A_2 and 100% A_2 cells are 8.5% and 6.2% respectively, consistent with previous reports.[18]

V_{OC} in OPVs is dictated by the diagonal band-gap of the system and disorder at the D:A interface; hence the broadening of charge transfer (CT) states in the corresponding ternary blend systems will play a crucial role in determining the voltage losses for a given diagonal band-gap.[44] The BHJ ternary solar cell could be modelled as having 2 diodes in parallel,[26] with each making an opposite contribution to the total current flowing through the device.

$$J_{total} = J_1(V) + J_2(V) \quad (1)$$

$$= (1-x)\left(J_{1_0}\exp\left(\frac{qV-E_1}{k_BT}\right) - J_{1_{ph}}\right) + (x)\left(J_{2_0}\exp\left(\frac{qV-E_2}{k_BT}\right) - J_{2_{ph}}\right) \quad (2)$$

Here, J_{total} is the total current density. J_1 and J_2 are the current densities of the A_1 and A_2 sub-cells, respectively. J_{1_0} and J_{2_0} are the maximum possible recombination current densities of the A_1 and A_2 sub-cells. $J_{1_{ph}}$ and $J_{2_{ph}}$ are the photocurrent densities for each respective sub-cell, and are taken as 16.1 mA cm^{-2} for a D:A_1 based OSC and 12 mA cm^{-2} for a D:A_2 based OSC, from experimental measurements of the short circuit currents under 1 sun illumination. E_1 and E_2 are the diagonal band-gaps ($HOMO_D - LUMO_A$) of A_1 and A_2 with D, respectively. x is the fraction of A_2 in the mixed devices, q is the electronic charge, V is the applied voltage, k_B is the Boltzmann constant and T is the temperature, assumed to be 300 K. The V_{OC} can then be calculated by numerically finding the value of V at which the total current density (J_{total}) is 0, with appropriate parameter values. Fig. 2a shows the fit according to a parallel-diode model. The model could fit the V_{OC}. However, due to the several assumptions pointed out in the introduction, it is not justifiable to use this model in disordered semiconductors.[27] So, we employ an analytical model based on population occupancy in Gaussian disordered semiconductors. The model assumes good mixing between A_1 and A_2. To confirm this, we performed the atomic force microscopy measurements shown in Fig. S1 (ESI†). We did not observe much difference in the roughness for a ternary system compared with two binary systems. To verify this, we calculated the diagonal band-gap experimentally using Marcus charge transfer (MCT) theory for different A_1:A_2 concentrations (Fig. S2, ESI†).[45] Then Vegard's law was used to fit the diagonal band-gap (E_{CT}) for different A_1:A_2 concentrations to calculate the bowing parameter.[46]

$$E_{CT}(x) = (1-x)E_{CT-1} + xE_{CT-2} - Bx(1-x) \quad (3)$$

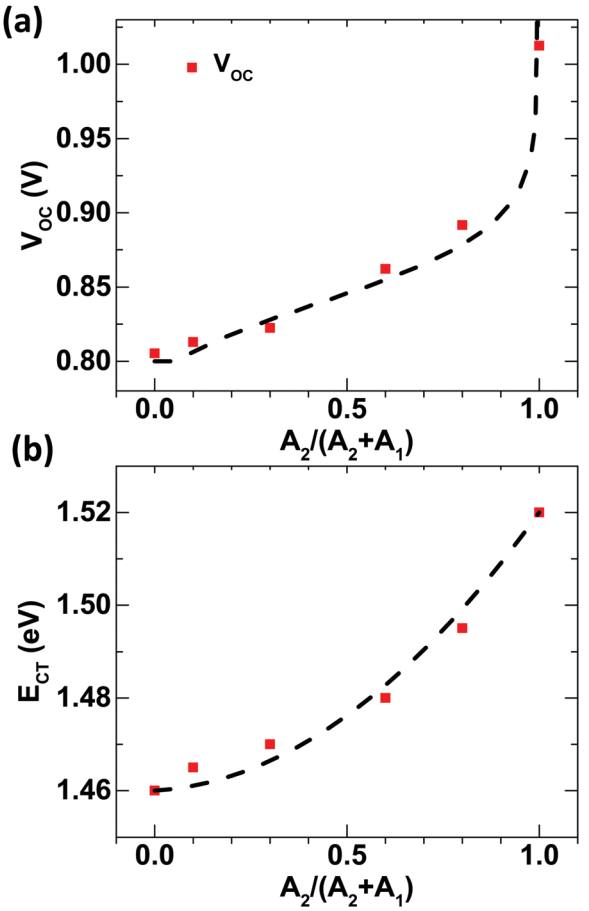

Fig. 2 Alloy composition vs. (a) changes in V_{OC} using the double-diode model (the dotted line represents the fitting of experimental V_{OC} values with eqn (2)) and (b) changes in the E_{CT} value of the BHJ alloy composition determined from sensitive EQE studies (the dotted line represents the fitting of experimental E_{CT} values with eqn (3).

where x is the fraction of A_2 in the mixture and B is the bowing parameter. E_{CT-1} and E_{CT-2} are the diagonal band-gaps of A_1 and A_2, respectively. The fitting of the experimentally calculated E_{CT} with the above equation is shown in Fig. 2b. The best fit is observed for a bowing parameter as low as 0.05. We note that this low value of the bowing parameter supports the good mixing assumption with least compositional disorder due to the alloying of different MSs[28,46] to be used in the population occupancy in the Gaussian disordered model for these ternary alloy systems.

It should be noted that V_{OC} is equal to the QFL spitting of hole and electron populations:

$$V_{OC} = E_{fe} - E_{fh} \quad (4)$$

Thus, in order to determine the QFL splitting (and hence, V_{OC}) for different ratios of A_1 *vs.* A_2, the population occupancy in the Gaussian disordered semiconductor system is estimated with the following equation:[47]

$$\rho(E) = \frac{P_0 \text{ or } N_0}{\sigma_{H \text{ or } L}\sqrt{2\pi}}\exp\left(-\frac{(E - E_{HOMO \text{ or } LUMO})^2}{2\sigma_{H \text{ or } L}{}^2}\right) \quad (5)$$

where σ_H (σ_L) is the broadening (disorder) of the DOS for the HOMO

(LUMO), P_0 (N_0) is the total site density of holes (electrons), and E_{HOMO} (E_{LUMO}) is the energy level of the donor (acceptor) material. The total site density in the MS is considered to be 10^{26} m^{-3}.[48] The value of $\sigma_H(\sigma_L)$ for D:A_1 and D:A_2 is calculated from temperature-dependent mobility (Fig. S5, ESI†) using a disorder-controlled transport mechanism. The details of this procedure are explained in ESI.† By using the temperature-dependent mobility, we found that the σ_H values are 69 meV and 63 meV for D:A_1 and D:A_2, respectively. Similarly, we found that σ_L varies from 72 meV to 78 meV for D:A_1 and D:A_2, respectively. Hence, it should be noted that there is no significant change in the energetic disorder with D:A_1 *vs.* D:A_2. Since this study focuses on devices with different acceptor concentrations, an effective DOS (ρ_e) for the electrons can be defined as:

$$\rho_e = R_{A1}\rho_{A1} + (1 - R_{A1}).\rho_{A2} \quad (6)$$

where R_{A1} (R_{A2}) is the ratio of acceptor A_1 (A_2) concentration to the total acceptor concentration, and ρ_{A1} and ρ_{A2} are the Gaussian density of states for A_1 and A_2, respectively. The effective DOS is then plotted for different $A_1:A_2$ ratios, as shown in Fig. 3a. It is interesting to see a monotonic change in the effective LUMO with the different $A_1:A_2$ ratios. It is observed that while A_1 and A_2 show a single Gaussian, the mixture of A_1:A_2 comprises both Gaussians, as can be clearly seen in Fig. 3a. It has previously been reported that A_1 and A_2 mix well[29,49] and do not alter the packing of the D MS, which suggests that the HOMO of D is not changed as a function of ternary composition. This is consistent with our observation of a low bowing parameter value for the ternary series of alloys used in this study. Hence, using the simulated effective HOMO/LUMO for alloys using eqn (5) and (6), the QFL of holes (E_{fh}) and electrons (E_{fe}) can be extracted from eqn (7) and (8):

$$\frac{p}{P_O} = \int_{-\infty}^{\infty} \frac{\rho_h}{P_0}.\frac{1}{\exp{(E-E_{fh})/kT} + 1}.dE \quad (7)$$

$$\frac{n}{N_O} = \int_{-\infty}^{\infty} \frac{\rho_e}{N_0}.\frac{1}{\exp{(E-E_{fe})/kT} + 1}.dE \quad (8)$$

where p/P_0 is the hole occupation density, n/N_0 is the electron occupation density, ρ_h and ρ_e = ρ(E) with e defined above (eqn (6)). The free hole carrier concentration (p) depends upon the absorption profile (Fig. S4, ESI†), internal quantum efficiency, illumination source (solar spectrum, AM1.5G), device thickness and carrier lifetime. These quantities are used to calculate p/P_0, as described in SI. The standard technique of minimum standard deviation (between experimentally and computationally obtained V_{OC}) was then used to obtain the value of n/N_0. This optimized value was further used for calculating E_{fe} and, thus, V_{OC} as a function of relative acceptor concentration. Further details of the methodology and parameter values (Table S4, ESI†) are provided in the ESI.† Fig. 3b shows that V_{OC} obtained from the Gaussian disordered state-filling model evidently reproduces the relative-acceptor-concentration-tuned experimental V_{OC} pretty well with respect to other models. Furthermore, the extracted values of QFL for holes and electrons are presented in Fig. 3c. It should be noted that while E_{fh} remains almost same for all concentrations, E_{fe} changes continuously. E_{fe} gets shallower as it moves from D:A_1 to D:A_2, as expected.

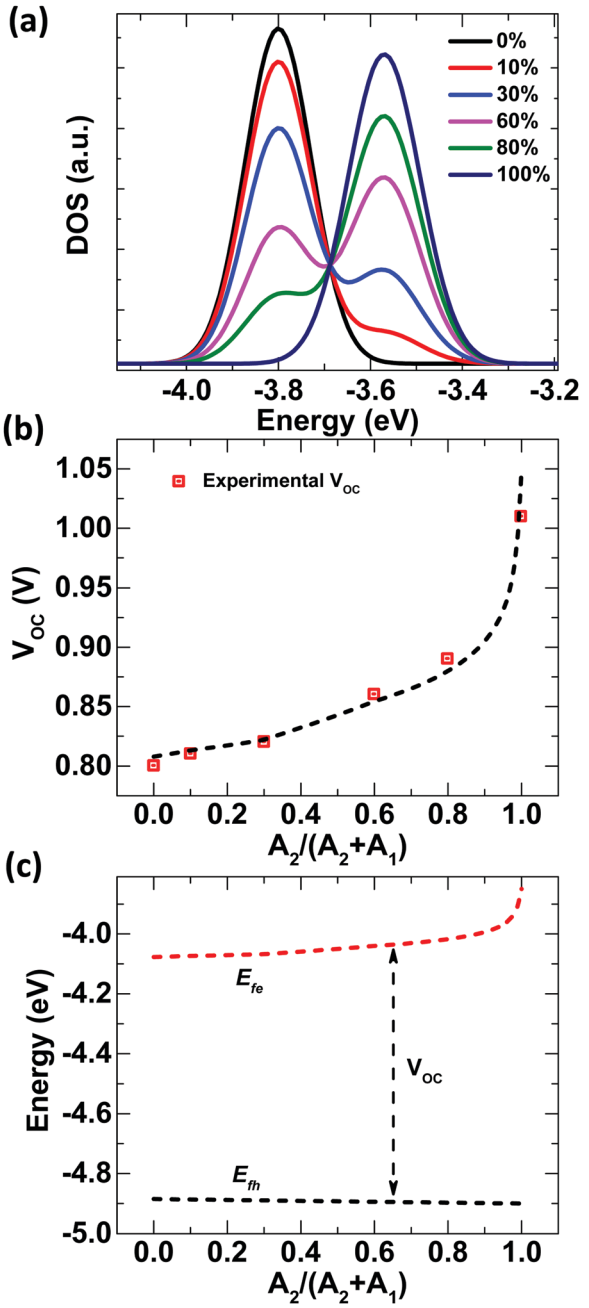

Fig. 3 Changes in DOSs for different A_1:A_2 concentrations plotted against energy using eqn (2) and eqn (3); (b) experimental V_{OC} values (red squares) fitted with a population occupancy DOS model (dashed line); and (c) QFL splitting for different $A_1:A_2$ ratios in D ternary blend solar cells, obtained from population occupancy in a Gaussian disorder model.

Discussion

V_{OC} depends directly upon the diagonal band-gap and the nature of the D:A interface. In these alloys we noted a continuous change in experimental V_{OC}. This experimental finding suggested that while alloying two acceptors, a new joint density of states is developed which is filled by light-induced carriers based on Fermi–Dirac statistics. The joint DOS for MSs is modeled using Bässler's Gaussian disordered model (eqn (5)).

Using this model, we could determine the QFL splitting for these alloys under 1 sun illumination conditions as a function of alloy composition, which suggested that energetic disorder is least influenced by alloying. To further understand the effect of molecular packing, we performed grazing incidence wide-angle X-ray scattering (GIWAXS) studies on D : A_1, D : A_1 : A_2 (1 : 0.5 : 0.5) and D:A_2 systems (Fig. S9, ESI†). GIWAXS studies indicate that there are only relatively minor changes in the molecular packing of the polymer donor, with the lamellar stacking peak (100) and π–π stacking peak (010) showing similar spacing. There is a slightly larger coherence length of these peaks for the case of D:A_1 compared to D:A_2 and D:A_1:A_2 (Table S4, ESI†), indicating slightly increased microstructural disorder for D in D:A_2 and D:A_1:A_2 thin-films with respect to D:A_1 blended films. However, in general, the influence of changes in molecular packing is expected to be insignificant and not to play a significant role in the observed monotonic change in V_{OC}. The formation of the joint DOS between A_1 and A_2 is the reason for the change in electron QFL with different concentrations of A_1:A_2. If we look at Fig. 3a closely, it is clearly observable that the LUMO of A_1 dominates up to 30% of A_2 with the presence of a small A_2 Gaussian on the shallower side. This is the reason even after adding 30% A_2, when the change in V_{OC} is dominated by the PCBM and very minor changes are obtained in V_{OC}. However, after 30% of A_2, the LUMO of A_2 starts to dominate with a small A_1 Gaussian on the deeper side and the change in V_{OC} is higher with 30% to 60% compared to 0% to 30%. Interestingly, the V_{OC} is still not dominated by A_2, because the light-induced charges have to fill the lower energy bands first, which are dominated by A_1. The prominent change in the from 80% to 100% A_2 concentration is because of the removal of the A_2 band on the lower energy side. At 100% A_2 concentration, light-induced charges will be directly filled within the Gaussian DOS of A_2 and hence a dramatic shift is observed in the electron QFL (or V_{OC}) from 80% to 100% of A_2 concentration. Hence, this detailed framework to analyze the BHJ OSCs not only allowed us to fit the experimental V_{OC} for the used compositions, but it also allows us to determine many useful parameters like charge transport physics (μ *vs.* T, Fig. S8, ESI†) and generation/recombination physics (TPV Fig. S3 and Table S2, ESI† used for the model) of OSCs correlated with effective energy levels along with the associated energetic disorder values.

Conclusions

In conclusion, QFL splitting as a function of the ternary alloy composition was studied for MSs, where a BHJ blend was prepared using one p-type and two n-type MSs. An analytical model based on the population occupancy of photoinduced fermions in a Gaussian disordered broadened joint DOS for an MS alloy is employed, with most of the parameters experimentally determined. A simple double-diode model or effective LUMO (*i.e.*, Vegard's law) model can explain the monotonic change in V_{OC} qualitatively, but these models can avoid good fitting and miss insights into the MSs physics. A monotonic change in V_{OC} is due to a monotonic change in E_{fe} while E_{fh} remains almost the same. Interestingly, a detailed Gaussian disorder with joint DOS based model fits the experimental V_{OC} values excellently and explains quantitatively that the deeper lying LUMO of A_1 dominates when determining V_{OC} in this ternary system, even at a relatively smaller concentration of D compared to A_2, since electrons start to fill from the lower energy state. These results were found to be consistent with the almost similar estimated energetic disorder (σ) values and negligible bowing parameter. Our model and transport studies can provide essential insights into light-induced QFL splitting for any general excitonic MS alloy system.

Conflicts of interest

There are no conflicts to declare.

Acknowledgements

We acknowledge Department of Science &Technology DST-AISRF and Global Challenges Research Fund (GCRF), SUNRISE for funding. DK acknowledges the Indo-Swedish joint project funded by DST-India (DST/INT/SWD/VR/P-20/2019) for funding support. We would like to acknowledge NCPRE IITB for providing the device fabrication and characterization facilities. This work was performed in part at the SAXS/WAXS beamline at the Australian Synchrotron, part of ANSTO.[43] We acknowledge Urvashi Bothra for preparing the sample for GIWAXS studies and Prof. Sir Richard H. Friend (Cambridge University, UK) for useful discussion and feedback. NJ acknowledges the Council of Scientific and Industrial Research (CSIR), India for the provision of a research fellowship.

References

1 M. Pope and C. E. Swenberg, *Electronic processes in organic crystals and polymers*, Oxford University Press on Demand, 1999.
2 T. Kirchartz, J. Nelson and U. Rau, *Phys. Rev. Appl.*, 2016, **5**, 054003.
3 Q. Liu, Y. Jiang, K. Jin, J. Qin, J. Xu, W. Li, J. Xiong, J. Liu, Z. Xiao and K. Sun, *Sci. Bull.*, 2020, **65**(4), 272–275.
4 J. Yao, T. Kirchartz, M. S. Vezie, M. A. Faist, W. Gong, Z. He, H. Wu, J. Troughton, T. Watson, D. Bryant and J. Nelson, *Phys. Rev. Appl.*, 2015, **4**, 014020.
5 M. Azzouzi, J. Yan, T. Kirchartz, K. Liu, J. Wang, H. Wu and J. Nelson, *Phys. Rev. X*, 2018, **8**, 031055.
6 F. Gao, W. Tress, J. Wang and O. Inganäs, *Phys. Rev. Lett.*, 2015, **114**, 128701.
7 N. C. Giebink, G. P. Wiederrecht, M. R. Wasielewski and S. R. Forrest, *Phys. Rev. B: Condens. Matter Mater. Phys.*, 2011, **83**, 195326.

8 N. C. Giebink, G. P. Wiederrecht, M. R. Wasielewski and S. R. Forrest, *Phys. Rev. B: Condens. Matter Mater. Phys.*, 2010, **82**, 155305.
9 A. D. Chepelianskii, J. Wang and R. H. Friend, *Phys. Rev. Lett.*, 2014, **112**, 126802.
10 N. Gasparini, X. Jiao, T. Heumueller, D. Baran, G. J. Matt, S. Fladischer, E. Spiecker, H. Ade, C. J. Brabec and T. Ameri, *Nat. Energy*, 2016, **1**, 16118.
11 S. Albert-Seifried, J. M. Hodgkiss, F. Laquai, H. A. Bronstein, C. K. Williams and R. H. Friend, *Phys. Rev. Lett.*, 2010, **105**, 195501.
12 I. Lange, J. C. Blakesley, J. Frisch, A. Vollmer, N. Koch and D. Neher, *Phys. Rev. Lett.*, 2011, **106**, 216402.
13 Z. Xiao, X. Jia and L. Ding, Ternary organic solar cells offer 14% power conversion efficiency, 2017.
14 H. Li, Z. Xiao, L. Ding and J. Wang, Thermostable single-junction organic solar cells with a power conversion efficiency of 14.62%, 2018.
15 N. Gasparini, L. Lucera, M. Salvador, M. Prosa, G. D. Spyropoulos, P. Kubis, H.-J. Egelhaaf, C. J. Brabec and T. Ameri, *Energy Environ. Sci.*, 2017, **10**, 885–892.
16 P. Xue, Y. Xiao, T. Li, S. Dai, B. Jia, K. Liu, J. Wang, X. Lu, R. P.-S. Han and X. Zhan, *J. Mater. Chem. A*, 2018, **6**, 24210–24215.
17 R. Sharma, S. Bhalerao and D. Gupta, *Org. Electron.*, 2016, **33**, 274–280.
18 W. Huang, E. Gann, N. Chandrasekaran, S. K.-K. Prasad, S.-Y. Chang, L. Thomsen, D. Kabra, J. M. Hodgkiss, Y.-B. Cheng, Y. Yang and C. R. McNeill, *Adv. Energy Mater.*, 2017, 7(11), 1602197.
19 R. Sharma, H. Lee, M. Seifrid, V. Gupta, G. C. Bazan and S. Yoo, *Sol. Energy*, 2020, **201**, 499–507.
20 C. Wang, X. Xu, W. Zhang, S. B. Dkhil, X. Meng, X. Liu, O. Margeat, A. Yartsev, W. Ma, J. Ackermann, E. Wang and M. Fahlman, *Nano Energy*, 2017, **37**, 24–31.
21 D. Baran, R. S. Ashraf, D. A. Hanifi, M. Abdelsamie, N. Gasparini, J. A. Röhr, S. Holliday, A. Wadsworth, S. Lockett, M. Neophytou, C. J.-M. Emmott, J. Nelson, C. J. Brabec, A. Amassian, A. Salleo, T. Kirchartz, J. R. Durrant and I. McCulloch, *Nat. Mater.*, 2016, **16**, 363.
22 R. Sharma, H. Lee, V. Gupta, H. Kim, M. Kumar, C. Sharma, S. Chand, S. Yoo and D. Gupta, *Org. Electron.*, 2016, **34**, 111–117.
23 X. Ma, A. Zeng, J. Gao, Z. Hu, C. Xu, J. H. Son, S. Y. Jeong, C. Zhang, M. Li, K. Wang, H. Yan, Z. Ma, Y. Wang, H. Y. Woo and F. Zhang, *Natl. Sci. Rev.*, 2020, 8.
24 W. J. Xu, X. L. Ma, J. H. Son, S. Y. Jeong, L. B. Niu, C. Y. Xu, S. P. Zhang, Z. J. Zhou, J. H. Gao, H. Y. Woo, J. Zhang, J. Wang and F. J. Zhang, *Small*, 2022, 18.
25 Z. H. Hu, J. Wang, Z. Wang, W. Gao, Q. S. An, M. Zhang, X. L. Ma, J. X. Wang, J. L. Miao, C. L. Yang and F. J. Zhang, *Nano Energy*, 2019, **55**, 424–432.
26 L. Yang, H. Zhou, S. C. Price and W. You, *J. Am. Chem. Soc.*, 2012, **134**, 5432–5435.
27 T. Ameri, P. Khoram, J. Min and C. J. Brabec, *Adv. Mater.*, 2013, **25**, 4245–4266.
28 M. Schwarze, W. Tress, B. Beyer, F. Gao, R. Scholz, C. Poelking, K. Ortstein, A. A. Günther, D. Kasemann, D. Andrienko and K. Leo, *Science*, 2016, **352**, 1446.
29 S. A. Mollinger, K. Vandewal and A. Salleo, *Adv. Energy Mater.*, 2015, **5**, 1501335.
30 N. Felekidis, E. Wang and M. Kemerink, *Energy Environ. Sci.*, 2016, **9**, 257–266.
31 Y. Cui, H. Yao, L. Hong, T. Zhang, Y. Xu, K. Xian, B. Gao, J. Qin, J. Zhang, Z. Wei and J. Hou, *Adv. Mater.*, 2019, 31.
32 T. T. To and S. Adams, *Phys. Chem. Chem. Phys.*, 2014, **16**, 4653–4663.
33 Y. Xie, F. Yang, Y. Li, M. A. Uddin, P. Bi, B. Fan, Y. Cai, X. Hao, H. Y. Woo, W. Li, F. Liu and Y. Sun, *Adv. Mater.*, 2018, **30**.
34 H. Bässler, *Phys. Status Solidi B*, 1981, **107**, 9–54.
35 S. M. Sze and K. K. Ng, *Physics of semiconductor devices*, Wiley-Interscience, Hoboken, N.J., 2007.
36 Q. S. An, J. Wang, W. Gao, X. L. Ma, Z. H. Hu, J. H. Gao, C. Y. Xu, M. H. Hao, X. L. Zhang, C. L. Yang and F. J. Zhang, *Sci. Bull.*, 2020, **65**, 538–545.
37 M. Kröger, S. Hamwi, J. Meyer, T. Riedl, W. Kowalsky and A. Kahn, *Appl. Phys. Lett.*, 2009, **95**, 123301.
38 Y. Zhou, C. Fuentes-Hernandez, J. Shim, J. Meyer, A. J. Giordano, H. Li, P. Winget, T. Papadopoulos, H. Cheun, J. Kim, M. Fenoll, A. Dindar, W. Haske, E. Najafabadi, T. M. Khan, H. Sojoudi, S. Barlow, S. Graham, J.-L. Brédas, S. R. Marder, A. Kahn and B. Kippelen, *Science*, 2012, **336**, 327–332.
39 S. Zhang, L. Ye, W. Zhao, D. Liu, H. Yao and J. Hou, *Macromolecules*, 2014, **47**, 4653–4659.
40 S. Park, J. Jeong, G. Hyun, M. Kim, H. Lee and Y. Yi, *Sci. Rep.*, 2016, **6**, 35262.
41 Z.-L. Guan, J. Bok Kim, Y.-L. Loo and A. Kahn, *J. Appl. Phys.*, 2011, **110**, 043719.
42 P. Cheng, Y. Li and X. Zhan, *Energy Environ. Sci.*, 2014, **7**, 2005–2011.
43 P. P. Khlyabich, B. Burkhart and B. C. Thompson, *J. Am. Chem. Soc.*, 2011, **133**, 14534–14537.
44 N. Jain, U. Bothra, D. Moghe, A. Sadhanala, R. H. Friend, C. R. McNeill and D. Kabra, *ACS Appl. Mater. Interfaces*, 2018, **10**, 44576–44582.
45 N. Jain, R. Sharma, S. Mahesh, D. Moghe, H. J. Snaith, S. Yoo and D. Kabra, *ACS Appl. Mater. Interfaces*, 2021, **13**, 60279–60287.
46 R. A. Street, D. Davies, P. P. Khlyabich, B. Burkhart and B. C. Thompson, *J. Am. Chem. Soc.*, 2013, **135**, 986–989.
47 G. Paasch and S. Scheinert, *J. Appl. Phys.*, 2010, **107**, 104501.
48 P. K. Nayak, G. Garcia-Belmonte, A. Kahn, J. Bisquert and D. Cahen, *Energy Environ. Sci.*, 2012, **5**, 6022–6039.
49 P. P. Khlyabich, B. Burkhart, A. E. Rudenko and B. C. Thompson, *Polymer*, 2013, **54**, 5267–5298.